# Traumatic brain injury – an investigation into shear waves interference effects

**Grand R. Joldes, Alesio L. Lanzara, Adam Wittek, Barry Doyle, Karol Miller**

Intelligent Systems for Medicine Laboratory, The University of Western Australia, Perth, Australia

**Abstract**

Traumatic brain injury (TBI) is one of the leading causes of long-term disability in both industrialised and developing countries around the world. It results in impaired and structural damage to the brain, caused by the application of external mechanical forces to the head. This paper aims to investigate the effect of shear wave interference as a key mechanism to TBI, by identifying localised regions of the brain exhibiting high strains in a comprehensive finite element (FE) head model.

We improved a magnetic resonance imaging (MRI) voxel-based mesh model of the head by introducing key meningeal membranes (dura mater, falx cerebri and tentorium cerebelli). We used this model to identify regions of interest through modal analysis and investigate the shear wave interference mechanism by transient modal dynamic analysis (TMDA) and the traditional explicit direct integration method (EDIM) under frontal impact loading scenarios. TMDA is a novel procedure for 3D head models and allows investigation into the influence of individual deformation modes on the overall system response.

Results show that falx cerebri and tentorium cerebelli play pivotal roles in the interference process, with some brain regions exhibiting amplification of strains 10-20ms after impact. These strains are seen to be higher than at the coup and counter-coup sites.

**Keywords:** Traumatic Brain Injury, shear waves, interference, transient modal dynamic analysis

## Introduction

Traumatic brain injury (TBI) is one of the leading causes of long-term disability in both industrialised and developing countries around the world. The World Health Organisation states that this type of debilitating injury will exceed many diseases

as the major cause of death and disability by the year 2020 [1]. What is this 'silent epidemic' [2] and why is it so damaging? TBI, also known as intracranial injury, results in temporarily or permanently impaired and structural damage to the brain, caused by the application of external mechanical forces to the head. These mechanical forces can be applied through various modes of excitation – rapid accelerations and decelerations, impact loads, inertial loads, blast waves and penetration-by-projectile. The environments these inputs can occur range from the extremely common – road traffic accidents, falls and other unintentional injuries, etc. to those affecting a particular subset of the population – contact sports, military activity, violence. The associated effects of TBI can range from mild (mTBI), which can lead to cognitive problems such as headaches, memory problems, mood swings and frustrations; to severe, which can lead to major causes of unconsciousness and persistent vegetative state after trauma. The latter is a result of diffuse axonal injury (DAI), involving damage of individual nerve cells (neurons) and splitting of the axonal connection between neurons due to traumatic shearing forces. It should come as no surprise now that there exists a vast amount of literature in the field of TBI, and the research dedicated to reducing its impact ranges from epidemiological studies [1] to the associated costs of traumatic brain injury [3, 4], to tissue/single cell-based work in order to detect the key molecular signatures of the injury [5]. The main problem is the inability to accurately define the relationship between kinetic inputs and subsequent brain injury and its associated effects. While clinicians and neuroscientists focus on pathological and physiological research, physicists and engineers use the principles of mechanics to study the physical phenomena involved in the TBI process to provide explanations for the cause of brain damage. Various methods have been employed to study the mechanics of brain injury, including animal and human cadaver experiments [6, 7], magnetic resonance imaging (MRI) and elastography (MRE) [8-11], physical modelling [12, 13] and mathematical modelling [14-16]. In particular, finite element (FE) modelling has become paramount in studying the mechanics of brain injury. A critical review of the state-of-the-art brain modelling and simulation for injury prevention together with practical guidelines for analysts creating finite element brain models have been recently published by Yang and King [17].

The stress and strain from FE solutions may be taken as a quantitative measure of tissue damage and correlated with pathological results from clinical and epidemiological investigations [18]. Once good correlations are proven and the FE model is well validated against experimental data specific to the injury mechanism being modelled, it may serve as a valuable tool for better understanding injury mechanisms, injury diagnosis and design of preventive technology.

According to current literature, DAI in humans is estimated to occur at maximum shear strains of 0.1 – 0.5 and strain rates of approximately 10 – 50/s [12, 13]. Further studies also suggest that the brain cells are considerably damaged at strains >0.10 and strain rates >10/s [18, 19].

The stresses and strains created by impact loading of the head are the result of dilatational (pressure) and distortional (shear) waves propagating throughout the brain [20]. Dilatational waves exhibit particle motion along the direction of propa-

gation while distortional waves display particle motion transverse to the direction of propagation. The two waves separate over time due to the large difference in wave speeds [21]. It is observed that the dilatational strains are approximately 1,000 times smaller than distortional strains, with minor differences between maximum shear strain and maximum principal strains in TBI events [22]. It is also important to note that key membranous structures, the falx cerebri (separating the cerebral hemispheres) and tentorium cerebelli (separating the cerebellum and occipital lobe), are seen to affect the shear wave propagation patterns in the brain due to the change in impedance, encouraging high reflection and attenuation [23].

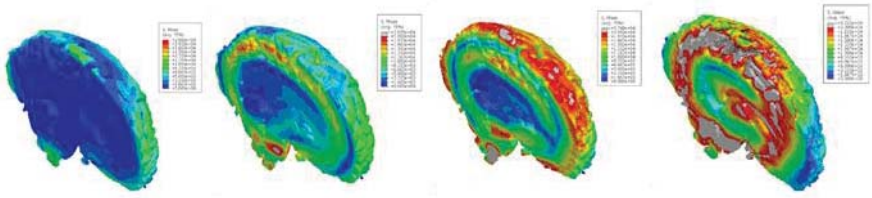

**Fig. 1.** Mid sagittal view of Von Mises stress distribution depicting spherically converging shear wave propagation (left to right) over 15ms.

Upon simulation of an angled frontal impact load to a 3D FE head of MRI resolution, Chen identifies spherically converging shear wavefronts, propagating from the skull boundary towards the inner regions of the brain [24] long after the pressure waves have subsided (Fig. 1). What was not investigated nor discussed however, was the response of the brain in an extended time domain, as travelling shear wavefronts of various frequencies interact with each other after reflection from substructures. These are referred to as interference effects, as superposition of shear wave amplitudes could create localised areas of high shear stress and strain, contributing to the TBI damage mechanism. To date, no direct investigation of shear wave interference has been made in the literature of TBI modelling.

This paper aims to investigate the effect of shear wave interference as a key mechanism to TBI, by identifying localised regions of the brain exhibiting high strains using a comprehensive FE head model.

## Finite Element Model of the Head

An MRI voxel-based FE mesh of the human head was obtained from Chen [24]. The very fine mesh makes it possible to capture stress wave propagation during impact loading. The model is capable of describing important geometrical features of the head due to the 1.33mm x 1.33mm x 1.30mm voxel size. A Laplacian mesh smoothing algorithm was used to achieve smooth outer surfaces and inner interfaces between tissues. The model's 1,061,799 elements and 1,101,599 nodes are separated into four different tissue types: white matter, grey matter, cerebrospinal fluid (CSF) and skull.

The profiles of the falx cerebri and tentorium cerebelli were carefully sculpted, by reassigning elements from the CSF, grey matter and white matter sets based on the geometry observed in coronal, sagittal and transverse MRI scans. The maximum thickness was two elements (2.66mm) in the falx cerebri and three elements (3.99mm) in the tentorium cerebelli, with at least 4 nodes shared between membrane elements. The thickness used is essential in effectively transmitting bending forces under dynamic simulations and is hence modelled slightly thicker than the approximate membrane thickness of 2mm [25]. The increased thickness is taken into consideration by scaling the Young's modulus of the membranes in order to obtain the correct bending rigidity.

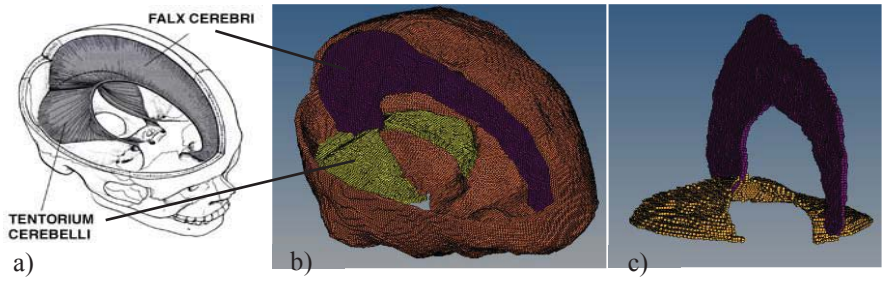


**Fig. 2.** a) The cranial cavity showing the falx cerebri and tentorium cerebelli; b) same view of the structures interior to the skull in the FE model; c) a frontal view of the membranes depicting the tent-like profile of the tentorium cerebelli.

The material data of the different tissues in the model were taken from [26]. The properties for the introduced Falx Cerebri and Tentorium Cerebelli are taken from literature and listed in Table 1. All materials are modelled as linear elastic, except the white and grey matter, which are modelled as hyper-viscoelastic (Neo-Hookean with Prony series viscoelasticity).

**Table 1.** Material properties for Falx Cerebri and Tentorium Cerebelli

| Tissue | Density $\rho$ [kg/m$^3$] | Bulk modulus K [Pa] | Short term shear modulus $G_0$ [Pa] | Reference |
|---|---|---|---|---|
| Falx Cerebri | 1130 | 4.47E+7* | 4.62E+6* | [25] |
| Tentorium Cerebelli | 1130 | 1.32E+7* | 1.37E+6* | |

* Scaled to account for difference in thickness

A fixed boundary condition is used at the head/neck junction. This allows us to capture the rotational motion of the brain, as a free boundary condition would lead mostly to linear motion of the head model. The pulse load shown in Fig. 3b is applied to the mid-frontal area of the model in the anterior-posterior direction as a uniformly distributed load over an area of 1,556 mm$^2$, shown in Fig. 3a [7].

a) 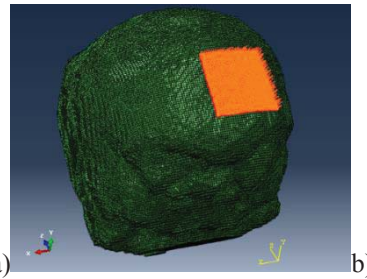 b) 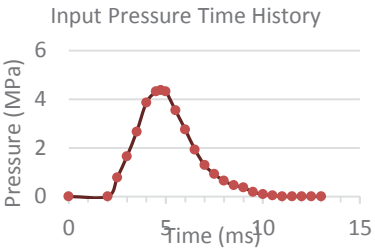


**Fig. 3.** a) The loaded area of the skull. b) Load pressure profile.

# Analysis Procedures

### Natural Frequency Extraction

The Natural Frequency Extraction step is used to extract the system's modes to be used for the subsequent modal dynamic analysis. The high-performance SIM-based linear dynamics architecture is enabled in this step to ensure that element and material damping factors related to the viscoelastic properties are taken into account in the subsequent modal dynamic analysis. The eigenvalues and the eigenvectors of the biomechanical head system are extracted in this procedure using the Lanczos eigensolver coupled with the SIM architecture [27]. The number of modes used in modal superposition is important in defining accurate dynamic response.

### Transient Modal Dynamic Analysis (TMDA)

The TMDA is used to investigate the shear wave interference process under various input loading profiles and compare the solution to the non-linear explicit dynamic analysis (EDIM).

While the natural frequency extraction step is computational expensive, finding the solution using TMDA is a relatively inexpensive procedure; therefore it is easy to investigate the behaviour for different loading pressure profiles.

### Explicit Dynamic Integration Method (EDIM)

The EDIM is used to investigate the shear wave interference while accounting for non-linear effects. It is ideally suited for large model analyses of high-speed dynamic events such as those seen in TBI. As the equations of motion for the body are integrated using the explicit central-difference integration rule, a large number of small time increments are used [27]. The integrity of the results generated using this method relies on the specified time increment being smaller than the stability

limit for the operator. This is based on the highest element frequency in the model, and the associated dilatational speeds observed.

## Results

The extracted modes in Table 5 shows that there is an approximate 10 Hz frequency span between the first 3-4 modes and thereafter, increasingly smaller increments until a span of 45 modes from 15-60 yields a frequency range of approximately 36 Hz. This is a by-product of the intricately complex structure of the head system. Although there are many complex modes of vibration, each contributing somewhat to the overall response, only a subset of these modes dominate the response of the system under impact loading. This information is contained within the modal effective mass in each kinematic direction, being dependent on the modal participation factors and the modal generalised mass of the system [27].

**Table 2.** Natural frequencies of the head model and the identified modes of interest.

| Mode Number | Frequency [Hz] | Effective Mass | | |
|---|---|---|---|---|
| | | X-Component | Y-Component | Z-Component |
| **1** | 47.948 | 6.91E-02 | **0.42853** | **1.0844** |
| 2 | 59.661 | 3.21E-07 | 6.87E-05 | 1.86E-04 |
| **3** | 60.981 | **0.176** | 4.91E-03 | 1.59E-02 |
| 4 | 69.707 | 2.71E-02 | 9.25E-04 | 7.81E-04 |
| **5** | 70.873 | 2.05E-02 | **0.12154** | **0.23524** |
| 6 | 74.858 | 9.30E-03 | 8.29E-04 | 1.25E-04 |
| 7 | 76.616 | 9.98E-03 | 1.30E-02 | 5.13E-03 |
| **8** | 79.156 | **0.40435** | 6.81E-03 | 5.64E-03 |
| 9 | 80.436 | 1.69E-03 | 1.70E-03 | 3.82E-02 |
| **10** | 81.132 | **0.11532** | 5.24E-04 | 2.16E-03 |
| **11** | 83.051 | **0.26127** | 5.31E-04 | 1.34E-02 |
| 12 | 83.685 | 1.34E-02 | 1.09E-02 | 4.75E-04 |
| … | … | … | … | … |
| 60 | 124.41 | 4.94E-07 | 3.62E-03 | 3.62E-04 |
| Total | | 2.3304 | 1.0706 | 1.7602 |
| Percentage of Total Mass | | 83% | 38% | 63% |

The effective mass in each kinematic direction for the first 60 modes is highest in the x direction, representing approximately 83% of the mass of the system. The y and z global kinematic directions return 38% and 63% respectively. The number of extracted modes is *not* sufficient to adequately represent the system under a

large range of transient inputs or impulse excitation. Approximately 90% of total mass in each kinematic direction is required for this.

The first natural frequency of the system is 48 Hz, contributing more than a third of the modal effective mass in the z direction. In fact, of particular interest in the y-z plane are the first and fifth modes for the first 60 modes. Lateral movement is dominated by modes 3, 8, 10, 11, 13 and 15. Figure 15 shows some of the associated mode shapes.

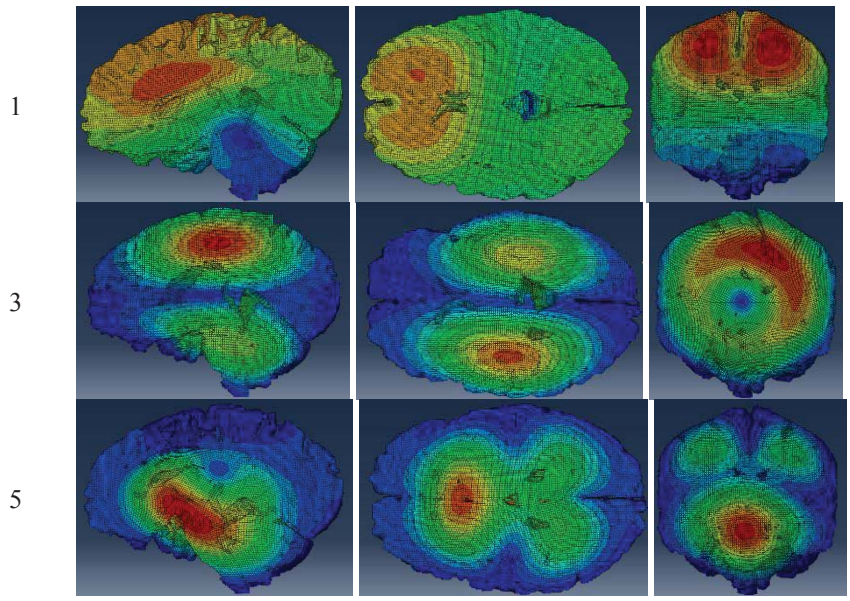


**Fig. 4.** The mode shapes (left column) viewed from the mid-sagittal, mid-transverse and mid-coronal cross sectional cuts of the brain. Regions of largest generalised displacements are red.

It is important to note however, that due to the rigidity of the skull, stress waves travel much faster here than in the soft tissues of the head. This is well represented by the spherically converging shear waves from impact loads, as a result of indirect loading induced by structural dynamical deformation of the skull. Hence, directionality of impacts may not be as significant in this study.

Regions of potential interference in brain tissue are identified by analysing perpendicular cross sections (sagittal, coronal and transverse planes) of the 3D generalised displacements and finding areas with the highest displacements. The maximum principal strains for these areas and the comparison with the coup site is presented in Table 3.

The dynamic response is mapped graphically through time in Fig. 5 to understand wave propagation behaviour. It is observed that wavefronts are not only converging from the outer boundary regions of the brain, but also propagating outwards from the falx cerebri. This creates two converging shear waves in each hemisphere, the focal points of which are the regions identified in the first mode –

the mid points of each parietal lobe. The maximum principal strain time history at these two locations is shown in Fig. 6. The dominant frequency is ~48Hz, corresponding to the first natural frequency. Strain amplification is observed, over a longer duration in the right hemisphere. The input load area slightly favours the left hemisphere, which explains the difference in local maximums.

**Table 3.** Regions of interest identified from the mode shapes

| Movement | Mode | Region Description | Max. Principal Strain | % difference from Coup |
|---|---|---|---|---|
| Anterior/Posterior | 1 | Left parietal lobe | 0.21 | -19% |
| | | Right parietal lobe | 0.21 | -19% |
| | | Mid cerebellar region | 0.26 | 0% |
| | 5 | Inferior region of the frontal lobe | 0.33 | +27% |
| Lateral | 3 | Mid-parietal lobe, directly right of falx cerebri insertion | 0.34 | +31% |
| | 8 | Cingulate gyrus, close to corpus callosum | 0.28 | +8% |
| | 13 | Right temporal lobe | 0.15 | -42% |

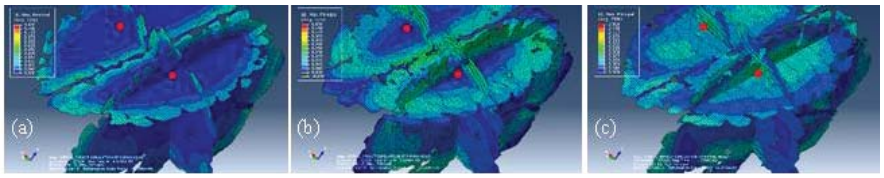


**Fig. 5.** Spherically converging shear waves in both cerebral hemispheres, shown at (a) 6.5ms (b) 8.5ms and (c) 10.5ms from the EDIM. Red dots denote the first two regions of interest.

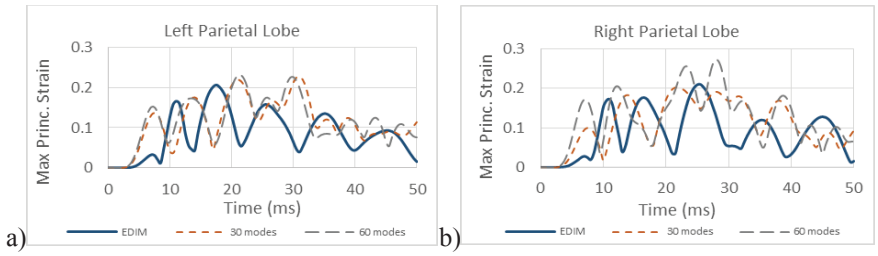


a) b)

**Fig. 6.** Maximum principal strain responses of a) the left, and b) right parietal lobes.

# Conclusions

This study successfully identifies regions in the brain which display higher strains than the coup and contre-coup sites for a frontal impact to the head. The wave patterns are strongly influenced by the falx cerebri and tentorium cerebelli.

The use of modal analysis to identify regions of interference is very effective, by taking into consideration the mode shapes (in strain and displacement) which have strong contributions to the overall response of the system. The TMDA, while not accounting for all solution nonlinearities, does provide an indication of interference effects, as shown by the comparison to the more accurate EDIM solution.

**Acknowledgments**

The authors thank Prof. Martin Ostoja-Starzewski and Ms. Ying Chen from University of Illinois at Urbana-Champaign for providing the mesh of the head.

# Bibliography

1. Hyder, A.A., et al., *The impact of traumatic brain injuries: a global perspective.* NeuroRehabilitation, 2007. **22**(5): p. 341-53.
2. Langlois, J.A., W. Rutland-Brown, and M.M. Wald, *The epidemiology and impact of traumatic brain injury: a brief overview.* J Head Trauma Rehabil, 2006. **21**(5): p. 375-8.
3. Humphreys, I., et al., *The costs of traumatic brain injury: a literature review.* Clinicoecon Outcomes Res, 2013. **5**: p. 281-7.
4. Ponsford, J.L., et al., *Costs of care after traumatic brain injury.* J Neurotrauma, 2013. **30**(17): p. 1498-505.
5. O'Dell, D.M., et al., *Traumatic brain injury alters the molecular fingerprint of TUNEL-positive cortical neurons In vivo: A single-cell analysis.* J Neurosci, 2000. **20**(13): p. 4821-8.
6. Meaney, D.F., et al., *Biomechanical analysis of experimental diffuse axonal injury.* J Neurotrauma, 1995. **12**(4): p. 689-94.
7. Nahum, A., R. Smith, and C. Ward, *Intracranial Pressure Dynamics During Head Impact.* Proc. 21st Stapp Car Crash Conf., 1977: p. 339-366.
8. Chatelin, S., et al., *Computation of axonal elongation in head trauma finite element simulation.* J Mech Behav Biomed Mater, 2011. **4**(8): p. 1905-19.
9. Manduca, A., et al., *Magnetic resonance elastography: non-invasive mapping of tissue elasticity.* Med Image Anal, 2001. **5**(4): p. 237-54.
10. Murphy, M.C., et al., *Analysis of time reduction methods for magnetic resonance elastography of the brain.* Magn Reson Imaging, 2010. **28**(10): p. 1514-24.
11. Okamoto, R.J., E.H. Clayton, and P.V. Bayly, *Viscoelastic properties of soft gels: comparison of magnetic resonance elastography and dynamic shear testing in the shear wave regime.* Phys Med Biol, 2011. **56**(19): p. 6379-400.
12. Margulies, S.S., L.E. Thibault, and T.A. Gennarelli, *Physical model simulations of brain injury in the primate.* J Biomech, 1990. **23**(8): p. 823-36.

13. Meaney, D.F. and L.E. Thibault, *Physical model studies of cortical brain deformation in response to high strain rate inertial loading*, in *International Conference on the Biomechanics of Impacts*1990: Lyon, France.
14. Holm, S. and R. Sinkus, *A unifying fractional wave equation for compressional and shear waves.* J Acoust Soc Am, 2010. **127**(1): p. 542-59.
15. Cloots, R.J., et al., *Biomechanics of traumatic brain injury: influences of the morphologic heterogeneities of the cerebral cortex.* Ann Biomed Eng, 2008. **36**(7): p. 1203-15.
16. Chadwick, P. and R.W. Ogden, *A theorem of tensor calculus and its application to isotropic elasticity*, 1971: School of Mathematics and Physics, University of East Anglia, Norwich.
17. Yang, K.H. and A.I. King, *Modeling of the Brain for Injury Simulation and Prevention*, in *Biomechanics of the Brain*, K. Miller, Editor 2011, Springer New York. p. 91-110.
18. Zhang, L., K.H. Yang, and A.I. King, *A proposed injury threshold for mild traumatic brain injury.* J Biomech Eng, 2004. **126**(2): p. 226-36.
19. Morrison, B., 3rd, et al., *A tissue level tolerance criterion for living brain developed with an in vitro model of traumatic mechanical loading.* Stapp Car Crash J, 2003. **47**: p. 93-105.
20. Holbourn, A.H.S., *Mechanics of head injuries.* Lancet, 1943. **2**: p. 438-441.
21. Kolsky, H., *Stress Waves in Solids*1963, New York: Dover Publications Inc.
22. Bradshaw, D.R.S. and C.L. Morley, *Pressure and shear responses in brain injury models*, U.o.S. ISVR, UK, Editor 2001.
23. Clayton, E.H., G.M. Genin, and P.V. Bayly, *Transmission, attenuation and reflection of shear waves in the human brain.* J R Soc Interface, 2012. **9**(76): p. 2899-910.
24. Chen, Y. and M. Ostoja-Starzewski, *MRI-based finite element modeling of head trauma: spherically focusing shear waves.* Acta Mechanica, 2010. **213**(1-2): p. 155-167.
25. Yoganandan, N., *Frontiers in Head and Neck Trauma: Clinical and Biomechanical*1998: IOS Press.
26. Chen, Y., *Biomechancial analysis of traumatic brain injury by MRI-based finite element modeling*, in *Mechanical Science & Engineering* 2011, University of Illinois at Urbana-Champaign: Illinois, USA.
27. DassaultSystèmes, *ABAQUS 6.13 Documentation*, 2013: Providence, RI, USA.